Anisotropy of Holder Gaussian random fields: characterization, estimation, and application to image textures

Frédéric J P Richard

Anisotropy of Holder Gaussian random fields: characterization, estimation, and application to image textures.

Frédéric J.P. Richard

Aix Marseille Univ, CNRS, Centrale Marseille, I2M, Marseille, France.

E-mail: frederic.richard@univ-amu.fr

Summary. The characterization and estimation of the Holder regularity of random fields has long been an important topic of Probability theory and Statistics. This notion of regularity has also been widely used in Image Analysis to measure the roughness of textures. However, such a measure is often not sufficient to characterize textures as it does account for their directional properties (*e.g.* isotropy and anisotropy). In this paper, we present an approach to further characterize directional properties associated to the Holder regularity of random fields. Using the spectral density, we define a notion of asymptotic topothesy which quantifies directional contributions of field high-frequencies to the Holder regularity. This notion is related to the topothesy function of the so-called anisotropic fractional Brownian fields, but is defined in a more generic framework of intrinsic random fields. We then propose a method based on multi-oriented quadratic variations to estimate this asymptotic topothesy. Eventually, we evaluate this method on synthetic data and apply it for the characterization of historical photographic papers.

Keywords: Holder regularity, anisotropy, fractional Brownian field, quadratic variations, texture analysis, photographic paper.

1. Introduction

In this paper, we focus on irregular Gaussian random fields (called Holder random fields) whose realizations are continuous but non-differentiable (see Section 2 for more details). The degree of Holder regularity of these fields is quantified by a parameter H (called the Holder index) in $(0, 1)$. Holderian fields include fractional Brownian fields ($i.e.$ multidimensional versions of fractional Brownian motions [22]), their anisotropic extensions [7, 8, 12, 15, 29] and some related stationary fields [13, 16]. They have been widely used in Image Analysis to model rough image textures from engineering domains as various as Medical Imaging [6, 10, 28, 30], Material Sciences [13, 16], or Hydrogeology [4]. The Holder index of these models has served for the quantification of texture roughness.

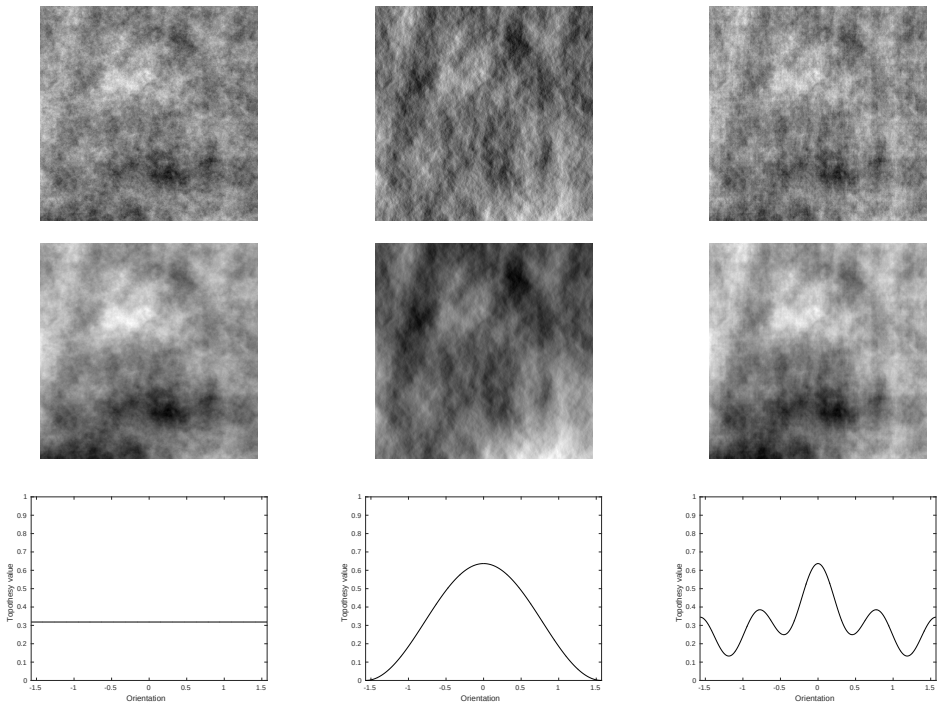

Fig. 1: Realizations of anisotropic fractional Brownian fields simulated using the turning-band method of [9]. Fields of first and second rows have Holder indices of 0.3 and 0.6, respectively. Fields of a same column have a topothesy function which is represented on the third row. Hurst functions of fields are constant and equal to the Holder index. All simulations were obtained using a same pseudo-random number sequence so as to highlight texture dissimilarities due to variations of the simulated fields.

However, this index is not always sufficient to characterize the texture aspect. In particular, since it is regardless of orientations, it does not account for directional properties of textures. This shortcoming is illustrated on Figure 1 with some simulated textures having both low and high Holder indices. From a regularity viewpoint, textures of the two different rows can be distinguished while those of a same row cannot. Differences between textures of a same row are only due to variations of their directional properties. In particular, the first texture of each row is isotropic (*i.e.* it has same aspect in all directions) whereas the second and third ones are anisotropic (*i.e.* their aspect varies depending on the direction).

The main motivation for this work is to set a description of textures that would not only account for their Holder regularity but also for relevant directional properties associated to this regularity. In that perspective, we first propose a characterization of the anisotropy of Holder fields. Then, we address the issue of estimating features derived from this characterization.

The anisotropy of Holder fields is often characterized through parameters of a specific model [8, 12, 15, 31]. As an example, anisotropic fractional Brownian fields (AFBF) introduced in [12] are d-dimensional Gaussian fields with stationary increments whose second-order properties are determined by a spectral density of a form (see Section 2 for details)

$$g_{\tau,\eta}(w) = \tau(\arg(w))|w|^{-2\eta(\arg(w))-d}. \quad (1)$$

Such a density depends on two functions τ and η called the topothesy and Hurst functions, respectively. By assumption, these functions are both even, positive, π-periodic, and bounded functions. Depending on the spectral orientation $\arg(w)$, they can be used to characterize directional properties of AFBF; visual effects induced by the topothesy function are illustrated on Figure 1. However, such a characterization is specific to a model. Moreover, it concerns all field frequencies (including its low frequencies) and is not exclusively associated to the field regularity. More generic characterizations which are intrinsically linked to a notion of regularity were developed in [1, 18, 33]. They rely upon the analysis of an anisotropic function space (typically, an anisotropic Besov space) by decomposition of fields into an appropriate basis (*e.g.* a basis of the hyperbolic wavelets).

In this paper, we investigate another characterization approach which is based on the field spectral density. In a generic framework of Holder random fields introduced in [29], we define a function, called the asymptotic topothesy, which quantifies directional contributions of high-frequencies of a field to its irregularity. This function is related to the topothesy of an AFBF. For such a field, field high-frequencies in directions where the Hurst function reaches a minimal value H are the largest. Due to these high-frequencies, the Holder index of the field is H (see Section 2 for details). The influence of these high-frequencies on the field regularity is further weighted by the topothesy function: the larger this function, the larger the high-frequencies and their contribution to the field regularity.

In a second part, we focus on the estimation of the asymptotic topothesy. This issue is both functional and non-parametric. It differs from the estimation issues that are usually tackled in the literature. Indeed, the analysis of directional features associated to random fields often reduces to the estimation of parameters of a specific anisotropic model. For instance, the estimation procedure of [31], which is an implementation of the anisotropy characterization by hyperbolic wavelets [1], targets the single parameter of a Gaussian operator scaling field. In [11, 30], it is devoted to the Hurst function of an AFBF. In these works, the estimation procedure is based on a Radon transform of images. Due to the discretization of this transform, the procedure can only be applied to the estimation of the

Hurst function in a few directions.

In [27, 28, 29], we have already investigated an estimation issue within the random field framework of this paper. In these works, an anisotropy analysis is developed using the so-called multi-oriented quadratic variations which are sums of squares of field increments computed in different directions. This analysis relies upon the estimation of a directional function which is asymptotically and linearly linked to quadratic variations. In this paper, we show that this directional function is indirectly related to the asymptotic topothesy through a convolution with a specific kernel that we analytically compute. We thus propose to recover the asymptotic topothesy of a field by solving an inverse problem associated to this convolution.

Eventually, we illustrate the interest of the asymptotic topothesy on an application to photographic papers. For the description of textures of these papers, we test a combination of two indices, an estimated Holder index and an anisotropy index derived from the estimated asymptotic topothesy.

2. Theoretical Framework

In this section, we first present a framework of intrinsic random fields, which is borrowed from [27, 28, 29]. In this framework, random fields are non-stationary with possible large polynomial trends. However, at some order, their increments fulfill a stationary assumption which will allow us to infer field properties from a single realization. We then recall the definition of Holder regularity and its spectral characterization. Eventually, we introduce a notion of asymptotic topothesy.

2.1. Intrinsic Random Fields

Intrinsic random fields are non-stationary fields whose increments are second-order stationary [14, 23]. Formally, they can be defined as follows.

DEFINITION 1. *Let $d \in \mathbb{N}\backslash\{0\}$, $M \in \mathbb{N}$, and Z a random field defined on $\mathbb{R}^d$. An increment field of order M of Z is a random field defined, for any $y \in \mathbb{R}^d$, as*

$$Z_{\lambda,x}(y) = \sum_{i=1}^{m} \lambda_i Z(x_i + y),$$

with some sets $(\lambda_i)_{i=1}^m$ of scalar values and $(x_i)_{i=1}^m$ of points in $\mathbb{R}^d$ satisfying the condition

$$\sum_{i=1}^{m} \lambda_i \, x_{i1}^{l_1} \cdots x_{id}^{l_d} = 0, \forall \; l \in \mathbb{N}^d, l_1 + \cdots + l_d \leq M. \tag{2}$$

A field is intrinsic of order M (or M-IRF) if its increment fields $Z_{\lambda,x}$ of order M are zero mean, and second-order stationary, i.e. for any y, $\mathbb{E}(Z_{\lambda,x}(y)) = 0$, and, for any y, z, $\mathbb{E}(Z_{\lambda,x}(y)Z_{\lambda,x}(z))$ only depends on $y - z$.

An M-IRF can model non-stationary fields with large polynomial trends. For $M = -1$ and $M = 0$, M-IRF correspond to usual stationary fields and fields with stationary increments, respectively.

Mean-square continuous M-IRFs are characterized by the so-called generalized covariances. These covariances are functions K for which

$$\mathbb{E}(Z_{\lambda,x}(0)Z_{\mu,y}(0)) = \sum_{i=1}^{m}\sum_{j=1}^{n} \lambda_i\, \mu_j K(x_i - y_j) \tag{3}$$

holds for any pair of M-increment fields $Z_{\lambda,x}$ and $Z_{\mu,y}$ of Z. They have a spectral representation [14, 17, 23, 29] which extends the Bochner representation of stationary field auto-covariances. For a large class of M-IRF, this representation is determined by a spectral density as follows.

Theorem 1 (Spectral representation). *Let M be an integer ≥ -1, and K a function of the form*

$$K(h) = \frac{1}{(2\pi)^d}\int_{\mathbb{R}^d} \left(\cos(\langle w, h\rangle) - \mathbf{1}_B(w) P_M(\langle w, h\rangle)\right) f(w)dw + Q(h), \tag{4}$$

where $P_M(t) = 1 - \frac{t^2}{2} + \cdots + \frac{(-1)^M}{(2M)!}t^{2M}$ if $M \geq 0$ and 0 if $M = -1$, $\mathbf{1}_B(w)$ is the indicator function of an arbitrary neighbourhood of 0, Q an arbitrary even polynomial of degree $\leq 2M$ if $M \geq 0$ and 0 if $M = -1$, and f is an even and positive function, called the spectral density, satisfying integrability conditions

$$\forall\, A > 0,\ \int_{|w|<A} |w|^{2M+2} f(w)dw < \infty \ \text{ and } \ \int_{|w|>A} f(w)dw < \infty. \tag{5}$$

Then, K is the generalized covariance of a M-IRF.

Example 1 (Anisotropic fractional Brownian fields). *AFBF, whose the density is given by Equation (1), are IRF of order $M \geq \overline{H} - 1$ with $\overline{H} = \operatorname{ess\,sup}_s \eta(s)$. In [27, 28, 29], anisotropic IRF were more generally defined by only assuming that their density f satisfies*

$$|w| > A \Rightarrow 0 \leq f(w) - g_{\tau,\eta}(w) \leq C|w|^{-2H-d-\gamma}, \tag{6}$$

for some positive constants A, C and a spectral density $g_{\tau,\eta}$ of the form (1). Such fields share properties of AFBF in the highest frequencies but are free to behave differently in the lowest ones.

Conditions in (5) are related to field properties at low and high frequencies, respectively. In particular, as the parameter M increases, the first condition becomes weaker, allowing the field to have larger low-frequencies.

In the representation (4) of an IRF Z, the integral can be decomposed into a sum of two integrals, one over low-frequencies ($|w| < A$) and another over high-frequencies ($|w| > A$), using an arbitrary cut-off A. The first integral is the generalized covariance of an IRF without high-frequency while the second one corresponds to the auto-covariance of a stationary random field. Hence, we can view an IRF Z as a sum of a smooth IRF T_A and a stationary random field $\tilde{Z}_A$.

In our application, we consider an image as a realization of an intrinsic random field Z. Moreover, we view the texture as an aspect of the image due to its high-frequencies. Hence, the texture is exclusively associated to the stationary part $\tilde{Z}_A$ of Z. The smooth IRF T_A produces on the image some low-frequency phenomena which are not of interest for the texture analysis.

2.2. Holder regularity

The Holder regularity of a field is defined as follows (see also [3]).

DEFINITION 2. *A field Z satisfies a uniform stochastic Hölder condition of order $\alpha \in (0,1)$ if, for any compact set $C \subset \mathbb{R}^d$, there exists an almost surely finite, positive random variable A such that the Hölder condition*

$$|Z(x) - Z(y)| \leq A|x - y|^{\alpha}. \tag{7}$$

holds for any $x, y \in C$, with probability one. If there exists $H \in (0,1)$ for which Condition (7) holds for any $\alpha < H$ but not for $\alpha > H$, then we say that Z is Holder of order H or H-Holder. The critical parameter H is called the Holder index.

Holder fields are well-suited for the modelling of images with rough textures. In such a modelling, we can interpret the texture as a visual effect of the field irregularity. Then, the texture roughness depends on the degree of the field regularity, and may be quantified from 0 to 1 by $1 - H$.

In the decomposition of an IRF Z into the sum of a low-frequency IRF T_A and a stationary field $\tilde{Z}_A$, the IRF T_A is indefinitely differentiable. Hence, the regularity of Z is only determined by the one of its high-frequency stationary field $\tilde{Z}_A$.

The Holder regularity is an asymptotic notion. For 0-IRF (and stationary fields), it is determined by the convergence speed of the semi-variogram at 0 (see [3] for instance) or,

equivalently, by the convergence speed of the spectral density at infinity. In [5], some useful conditions were established on the spectral density to characterize the Holder regularity of an arbitrary IRF.

PROPOSITION 1 (PROPOSITIONS 2.1.6 AND 2.1.7 OF [5]). *Let Z be a mean square continuous Gaussian IRF with a spectral density f, and $H \in (0,1)$.*
(i) If for any $0 < \alpha < H$, there exist two positive constants A_1 and B_1 such that for almost all $w \in \mathbb{R}^d$

$$|w| \geq A_1 \Rightarrow f(w) \leq B_1 |w|^{-2\alpha - d}, \tag{8}$$

then the field Z is Holder of order $\geq H$.
(ii) If, for any $H < \beta < 1$, there exist two positive constants A_2 and B_2 and a positive measure subset E of $[0, 2\pi)^{d-1}$ such that

$$|w| \geq A_2 \text{ and } \arg(w) \in E \Rightarrow f(w) \geq B_2 |w|^{-2\beta - d}, \tag{9}$$

then the field Z is Holder of order $\leq H$.
(iii) If conditions (8) and (9) both hold, then the field Z is H-Hölder.

Let us apply this proposition to a field Z whose spectral density f fulfills Equation (6) for a spectral density $g_{\tau,\eta}$. Condition (8) holds for

$$H = \operatorname{ess} \inf_{s \in [0,2\pi)^{d-1}} \eta(s) \in (0,1). \tag{10}$$

Assume that the set

$$E_0 = \{s \in [0,2\pi)^{d-1}, \tau(s) \neq 0, \eta(s) = H\} \tag{11}$$

is of positive measure. Then, Condition (9) holds for some set $E \subset E_0$. Therefore, the field Z is H-Hölder.

2.3. Asymptotical Topothesy

Let us assume that the density of a field fulfils Condition (6) for some $H \in (0,1)$. Then, there exists a non-negative and bounded function τ^* defined for any direction s of $[0,2\pi)^{d-1}$ as

$$\tau^*(s) = \lim_{\rho \to +\infty} f(\rho s) \rho^{2H+d}. \tag{12}$$

We can notice that $\tau^*(s) = \tau(s)$ whenever $\eta(s) = H$ and 0 otherwise. We will call the function τ^* the asymptotic topothesy. Basically, it gives a measure of the speed at which the spectral density converges to 0 at infinity in each direction. Intuitively, such a measure

quantifies the magnitude of field high-frequencies: the larger τ^* in a direction, the slower the density convergence and the larger high-frequencies in that direction. Since τ^* is bounded, the density convergence occurs at a speed which is not slower than a reference speed of order ρ^{-2H-d}. According to Proposition 1 (i), this implies that the Holder index of the field cannot be below H. In directions s where $\tau^*(s) = 0$ the convergence speed is faster than any speed of order ρ^{-2H-d}. Hence, in these directions, the condition of Proposition 1 (ii) is not satisfied. This means that high-frequencies of these directions are not large enough to make the Holder index of the field as low as H. By contrast, the convergence speed is of order ρ^{-2H-2} in directions of the set

$$E_0 = \{s, \tau^*(s) > 0\}. \tag{13}$$

On E_0, the condition of Proposition 1 (ii) holds, which implies that the Holder index is exactly H. In other words, high-frequencies in directions of E_0 contribute to the field irregularity. Their contributions are further weighted by the asymptotic topothesy: the larger τ^* in a direction of E_0, the larger the contribution of high-frequencies to the field irregularity.

We will say that the field texture is isotropic when these contributions are uniform (*i.e.* the asymptotic topothesy is constant), and anisotropic when they are not. Let us outline that these notions of isotropy and anisotropy describe high-frequencies of the field, and are intrinsically related to its irregularity.

Next, we state a proposition showing how the asymptotic topothesy characterizes the correlation structure of the field high-frequencies.

PROPOSITION 2. *Let Z be an IRF whose density f fulfills Condition (6) for some Hurst index $H \in (0,1)$ and asymptotic topothesy τ^* (see Equation (12)). Then, as $A \to +\infty$, for any $x \in \mathbb{R}^d$,*

$$K_{A,f}(x) - K_{A,f^*}(x) = o(A^{-2H}), \tag{14}$$

where $K_{A,f}$ and K_{A,f^*} are two auto-covariances defined by

$$K_{A,g}(x) = \frac{1}{(2\pi)^d} \int_{|w|>A} e^{i\langle x,w\rangle} g(w) dw \quad \text{and} \quad f^*(w) = \tau^*(\arg(w))|w|^{-2H-d}. \tag{15}$$

In this proposition, $K_{A,f}$ corresponds to the auto-covariance of the high-frequency stationary field $\tilde{Z}_A$ of a decomposition of Z. Equation (14) means that, when A tends to ∞, the correlation structure of this field gets approximately the same as the one of another stationary field whose auto-covariance K_A^* only depends on the Hurst index and the asymptotic topothesy.

3. Estimation Method

In this section, we address the issue of the estimation of the asymptotic topothesy.

3.1. Multi-oriented Quadratic variations

Multi-oriented quadratic variations were introduced in [29] to construct isotropy tests, and further used in [27, 28] to develop anisotropy indices. The definition of these variations is based on the computation of image increments. These increments give some information about image variations at highest observed scales which are not marked by trends. Moreover, as they are computed in different orientations, they provide us with relevant directional information.

Let us assume that an image is a realization of a random field Z on a grid $[\![1, N]\!]^d$. Let us denote by $Z^N[m] = Z(m/N)$ the image intensity at position $m \in \mathbb{Z}^d$. Given a vector u in $\mathbb{Z}^d$, increments in direction $\arg(u)$ at scale $|u|$ are obtained by a discrete convolution

$$\forall m \in \mathbb{Z}^d, V_u^N[m] = \sum_{k \in \mathbb{Z}^2} v[k] Z^N[m - T_u k], \tag{16}$$

with an appropriate convolution kernel v and a transform T_u which is a combination of a rotation of angle $\arg(u)$ and a rescaling of factor $|u|$. In dimension 2 ($d = 2$), transforms T_u are defined as

$$T_u = \begin{pmatrix} u_1 & -u_2 \\ u_2 & u_1 \end{pmatrix} = |u| \begin{pmatrix} \cos(\arg(u)) & -\sin(\arg(u)) \\ \sin(\arg(u)) & \cos(\arg(u)) \end{pmatrix},$$

The kernel is chosen so as to ensure that the convolution annihilates any polynomial of a predefined order K (kernel of order K) [29].

EXAMPLE 2. *Some two-dimensional kernels selected in [29] for their optimality are given for $L \in \mathbb{N}\backslash\{0\}$ by*

$$v[l_1, l_2] = (-1)^{l_1} \binom{L}{l_1}, \tag{17}$$

if $(l_1, l_2) \in [\![0, L]\!] \times \{0\}$ and 0 otherwise, $\binom{n}{k}$ standing for the binomial coefficient. Such a kernel is of order $K = L - 1$.

The information provided by increments are summarized into a single random variable called quadratic variations

$$W_u^N = \frac{1}{N_e} \sum_{m \in \mathcal{E}_N} (V_u^N[m])^2, \tag{18}$$

where $\mathcal{E}_N$ is a set of cardinal N_e containing positions m where increments can be computed on grid points. To get information at different scales and orientations, we compute

quadratic variations for different vectors u indexed in a set $\mathcal{I}$ of size n_I. We gather all these variations into a single random vector $Y^N = \left(\log(W_{u_k}^N)\right)_{k\in\mathcal{I}}$ of log-variations. The following theorem specifies the asymptotic probability distribution of Y^N.

THEOREM 2. *For some integer $M \geq -1$, let Z be a mean-square continuous Gaussian M-IRF. Assume that its spectral density f fulfills Condition (6) for some $H \in (0,1)$. Let τ^* asymptotic topothesy defined by Equation (12). Consider a log-variation vector Y^N constructed using a kernel v of order $K > M$ and $K \geq M/2 + d/4$ if $d > 4$. For all $i \in \mathcal{I}$, define random variables ϵ_i^N such that*

$$Y_i^N = H\ x_i^N + \log(\beta_{H,\tau^*}(\arg(u_i))) + \epsilon_i^N, \tag{19}$$

with $x_i^N = \log(|u_i|^2/N)$ and

$$\beta_{H,\tau^*}(\theta) = \frac{1}{(2\pi)^d} \int_{[0,2\pi)^{d-1}} \tau^*(\varphi)\ \Gamma_{H,v}(\theta - \varphi)\ d\varphi = \tau^* \circledast \Gamma_{H,v}(\theta), \tag{20}$$

where $\circledast$ stands for a circular convolution product over $[0,2\pi)^{d-1}$, and $\Gamma_{H,v}$ is defined by

$$\Gamma_{H,v}(\theta) = \int_{\mathbb{R}^+} |\hat{v}\,(\rho\theta)|^2\, \rho^{-2H-1} d\rho, \tag{21}$$

with $\hat{v}$ the discrete Fourier transform of v. Then, as N tends to $+\infty$, the random vector $(N^{\frac{d}{2}}\epsilon_i^N)_{i\in\mathcal{I}}$ tends in distribution to a centred Gaussian vector.

This theorem is proved in [29] (Theorem 3.4). The expression of β_{H,τ^*} in Equation (20) was slightly changed to highlight a convolution product.

3.2. Inverse Problem

Theorem 2 shows some interesting links between log-variations and the asymptotic topothesy τ^* we aim to estimate. According to Equation (19), the expectation of these variations is linearly related to the Hurst index. In this linear relationship, the intercept function β_{H,τ^*} depends both on the Hurst index and the asymptotic topothesy. More precisely, due to Equation (20), it is given by a circular convolution product of τ^* and a function $\Gamma_{H,v}$ defined by Equation (21). Hence, we propose to find τ^* by inverting this convolution product. Next, we develop a method in dimension $d = 2$.

Let $\{\theta_j\}_{j\in\mathcal{J}}$ be an indexed subset of $[0,2\pi)$ composed by arguments of vectors $\{u_i\}_{i\in\mathcal{I}}$. Assume that we have some estimates $\tilde{\beta}_j$ of $\beta_{H,\tau^*}(\theta_j)$ for $j \in \mathcal{J}$, and an estimate $\tilde{H}$ of the Hurst index H. Consider the ordinary least square criterion

$$C_{\tilde{H},\tilde{\beta}}(\tau) = \sum_{j\in\mathcal{J}} \left(\tilde{\beta}_j - \Gamma_{\tilde{H},v} \circledast \tau(\theta_j)\right)^2, \tag{22}$$

One way to find the topothesy τ^* would be to minimize this criterion over the space of π-periodic functions of $L^2([0,2\pi))$. Unfortunately, this minimization problem is ill-posed; as we shall see in practice, it lacks stability, especially when H is close to 1.

So as to fix this issue, we propose to minimize an appropriate penalized least square criterion. To define this criterion, we first expand π-periodic functions τ of $L^2([0,2\pi))$ in a cosine/sine basis:

$$\forall \theta \in [0,2\pi), \tau(\theta) = \tau_0 + \sum_{m\geq 1} \tau_{1,m}\cos(2m\theta) + \tau_{2,m}\sin(2m\theta), \tag{23}$$

for some scalar coefficients $\{\tau_0, \tau_{1,m}, \tau_{2,m}, m \geq 1\}$. From now on, we will use the same notation τ for the function and the vector formed by its expansion coefficients. We then consider a Sobolev space formed by functions τ whose coefficients satisfy

$$|\tau|_W^2 := \tau_0^2 + \sum_{m\geq 1}(1+m^2)(\tau_{1,m}^2 + \tau_{2,m}^2) < +\infty. \tag{24}$$

The mapping $|\cdot|_W$ defined above is a norm on the space W. Functions of W are continuously differentiable.

Now, in order to recover the topothesy, we solve the following inverse problem: find the function τ_λ^* which minimizes over the space W the penalized least square criterion

$$\tilde{C}_{\tilde{H},\tilde{\beta},\lambda}(\tau) = C_{\tilde{H},\tilde{\beta}}(\tau) + \lambda|\tau - \tau_0|_W^2, \tag{25}$$

with $\tau_0 = \int_{[0,\pi)} \tau(\theta)d\theta$ and $\lambda > 0$.

The second term of this criterion can also be written

$$|\tau - \overline{\tau}|_W^2 = \sum_{m\geq 1}(1+m^2)(\tau_{1,m}^2 + \tau_{2,m}^2).$$

It penalizes variations of components of τ with weights $(1+m^2)$ that strengthen as their frequency increases. It constrains the solution to remain as close as possible to a constant function. The parameter λ sets a trade-off between this prior constraint on the solution and the fidelity of the recovered τ^* to observations (as measured by $C_{\tilde{H},\tilde{\beta}}$). In Section 3.3, we will present a method to set this parameter optimally.

3.3. Numerical Resolution

In order to minimize the criterion in Equation (25), we first need to evaluate the convolution with $\Gamma_{H,v}$ in the expression of the least square criterion. The following proposition gives a computable expression of this convolution in cases when filters v are mono-directional in dimension 2 (see Example 2).

PROPOSITION 3. *Let v be a mono-directional increment filter, i.e. v is of the form $v[l_1, l_2] = v_1[l_1]$, for $(l_1, l_2) \in [\![0, L]\!] \times \{0\}$ and 0 otherwise. Then, for $\theta \in [0, 2\pi)$,*

$$\beta_{H,\tau^*}(\theta) = \tau^* \circledast \Gamma_{H,v}(\theta) = \gamma_{H,v}\ \tau^* \circledast \mu_H(\theta), \tag{26}$$

where

$$\forall\, \theta \in \mathbb{R},\ \mu_H(\varphi) = |\cos(\varphi)|^{2H} \quad \text{and} \quad \gamma_{H,v} = 2\int_{\mathbb{R}+} |\hat{v}_1(\rho)|^2 \rho^{-2H-1} d\rho. \tag{27}$$

To apply this proposition, we will not evaluate the constant $\gamma_{H,v}$, but only the convolution product $\tau^* \circledast \mu_H$. Consequently, we will just estimate the topothesy up to a constant. However, as we shall see in Section 5, this is not a real matter for our applications since we will only use a normalized version of the asymptotic topothesy.

To solve the minimization problem, we approximate the solution in a finite-dimensional subspace W^A of W defined by

$$W^A = \left\{ \tau \in W, \tau(\theta) = \tau_0 + \sum_{m=1}^{A} \tau_{1,m} \cos(2m\theta) + \tau_{2,m} \sin(2m\theta), \forall\, \theta \right\} \tag{28}$$

for some positive integer A.

On W^A, the penalized criterion can be expressed as

$$\tilde{C}^A_{\tilde{H},\tilde{\beta},\lambda}(\tau) = |L_{\tilde{H}}\tau - \tilde{\beta}|^2 + \lambda\, \tau^T R \tau, \tag{29}$$

where $\tilde{\beta} = (\tilde{\beta}_1, \cdots, \tilde{\beta}_{n_J})^T$ is a column vector of estimates, $\tau = (\tau_0, \tau_{1,1}, \tau_{2,1}, \cdots, \tau_{1,A}, \tau_{2,A})^T$ a vector of coefficients of τ, $L_{\widehat{H}}$ a matrix of size $n_J \times (2A+1)$ whose kth row is given by

$$\left(\hat{\mu}_{\widehat{H}}[0], \hat{\mu}_{\widehat{H}}[1]\cos(\theta_k), \hat{\mu}_{\widehat{H}}[1]\sin(\theta_k), \cdots, \hat{\mu}_{\widehat{H}}[A]\cos(A\theta_k), \hat{\mu}_{\widehat{H}}[A]\sin(A\theta_k)\right),$$

with $\theta_k = \arg(u_k)$, $\hat{\mu}_H$ the discrete Fourier transform of the function μ_H defined by Equation (27), and R a diagonal matrix of size $(2A+1)\times(2A+1)$ whose terms on the diagonal are $(0, 2, 2, \cdots, (1+A^2), (1+A^2))$.

The minimum of the approximated criterion $\tilde{C}^A_{\widehat{H},\widehat{\beta},\lambda}$ is reached at

$$\tilde{\tau}^*_\lambda = (L^T_{\tilde{H}} L_{\tilde{H}} + \lambda R)^{-1} L^T_{\tilde{H}} \tilde{\beta}. \tag{30}$$

To compute this solution, estimates $\tilde{H}$ and $\tilde{\beta}$ of H and β are required. In our implementation, we took ordinary least square estimates of parameters of the linear model (19) [27, 28, 29]. Using the Δ-method and Theorem 2, it could be shown that these estimates are both unbiased and asymptotically Gaussian.

3.4. Choice of λ.

The solution $\tilde{\tau}^*_\lambda$ given by Equation (30) is intended to approach the solution τ^* of the linear system

$$L_H \tau = \beta \tag{31}$$

using some estimates $\tilde{\beta}$ and $\tilde{H}$ of β and H, respectively.

Next, we give some bounds for the relative bias and variance of this estimation. To get these bounds, we neglect the effect of estimating H, and set $L_H \simeq L_{\tilde{H}}$.

THEOREM 3. *Let $\mathrm{V}(\tilde{\tau}^*_\lambda)$ and $\mathrm{V}(\tilde{\beta})$ be covariance matrices of the estimate vectors $\tilde{\tau}^*_\lambda$ and $\tilde{\beta}$, respectively. Let τ^* be the solution of the linear system (31). Let ν_- and ν_+ be the lowest and highest eigenvalues of the matrix $L_H^T L_H$, respectively. Set $\kappa = \frac{\nu_+}{\nu_-}$ the 2-norm condition number of the matrix $L_H^T L_H$. Then, the relative bias and standard deviation of $\tilde{\tau}^*_\lambda$ taken as an estimator of τ^* are bounded as follows.*

$$\mathrm{BIAS} = \frac{|\mathbb{E}(\tilde{\tau}^*_\lambda) - \tau^*|}{|\tau^*|} \leq \frac{\lambda\,(1+A^2)}{\lambda + \nu_-}, \tag{32}$$

$$\mathrm{STD} = \frac{\sqrt{\mathrm{trace}(\mathrm{V}(\tilde{\tau}^*_\lambda))}}{|\tau^*|} \leq \frac{\kappa\,\sqrt{\nu_-}\,\sqrt{\mathrm{trace}(\mathrm{V}(\tilde{\beta}))}}{|\beta|\,(\lambda+\nu_-)}. \tag{33}$$

Using this theorem, we can find an optimal value of λ minimizing the bound of the relative mean square error.

COROLLARY 1. *In the estimation of τ^* by $\tilde{\tau}^*_\lambda$, the relative mean square error*

$$\mathrm{RMSE}(\lambda) = \mathbb{E}\left(\frac{|\tilde{\tau}^*_\lambda - \tau^*|^2}{|\tau^*|^2}\right)$$

is bounded by

$$g(\lambda) = \frac{1}{(\lambda+\nu_-)^2}\left((1+A^2)^2\lambda^2 + \frac{\kappa^2\nu_-\mathrm{trace}(\mathrm{V}(\tilde{\beta}))}{|\beta|^2}\right),$$

for all $\lambda > 0$. This function reaches a global minimum at

$$\lambda^* = \frac{\kappa\,\mathrm{trace}(\mathrm{V}(\tilde{\beta}))}{|\beta|^2\,(1+A^2)}. \tag{34}$$

In practice, we set the penalization weight λ to λ^*. According to Equation (34), this implies that the penalization hardens as the condition number of $L_H^T L_H$ or variances of estimators $\tilde{\beta}$ increases. Such an increase occurs when the Hurst index H gets close to 1 (see Section 4).

4. Numerical Study

We evaluated our estimation procedure using 10000 realizations on a grid of size 800×800 of anisotropic fractional Brownian fields (see definition in Example 1). These realizations were simulated using the turning-band method developed in [9]. The Hurst function η of each simulated field was set to a constant, which was sampled from a uniform distribution on $(0.05, 0.95)$. Its topothesy was defined in the approximation space $W^{\bar{A}}$ for $\bar{A} = 47$ (see Equation (28)). Its expansion coefficients $\tau_{i,k}$ were sampled from independent centered Gaussian distributions of decreasing variances $\frac{1}{(1+k^2)}$. We set the coefficient $\tau_0 = \sum_{k=1}^{A} |\tau_{1,k}| + |\tau_{2,k}|$ so as to ensure that the topothesy was non-negative.

On each simulated field, we computed increments and quadratic variations (see Equations (16) and (18)) at scales $|u|$ and in directions $\arg(u)$ prescribed by all vectors u of the set $\{v \in \mathbb{N} \times \mathbb{Z}, |v| \in [1, 20]\}$ for which there exists at least another v in the same set with $\arg(v) = \arg(u)$. To compute increments, we used a kernel v of the form (17) with $L = 2$. Next, using these quadratic variations, we could estimate the intercept function β_{H,τ^*} of Equation (20) at 96 different angles. Eventually, we computed several estimates of the asymptotic topothesy by solving Equation (30) in approximation spaces W^A of different dimensions $2A+1$ for $A \in [\![1, \bar{A}]\!]$. In Equation (30), the parameter λ was set to the optimal value λ^* given by Equation (34). For comparison, we also computed solutions obtained without penalization for $\lambda = 0$.

For each type of estimation, we evaluated the mean square error (MSE) by averaging squares of the quadratic distances between the estimated and true topothesy. To decompose this error, we further evaluated approximation and estimation errors. The first error was obtained by averaging square distances between the original topothesy in the space $W^{\bar{A}}$ and its projection into an approximation space W^A of lower dimension. The second one was obtained by averaging the square distance between the true and estimated topothesy in the space W^A. These errors are plotted on Figure 2; they are expressed in percent of the mean square norm of true topothesy function.

As the dimension of the approximation space was increased, the estimation error increased for both methods (with and without penalization). At lowest dimensions, the increase of these errors was compensated for by a decrease of approximation errors, leading to a decrease of MSE. Above a critical dimension, estimation errors became predominant and MSE started to increase. This critical dimension was only $A = 5$ without penalization and $A = 19$ with penalization. At this dimension, the minimum reached by the MSE was higher for the method without penalization (2.7%) than for the penalization one (1.5%). After

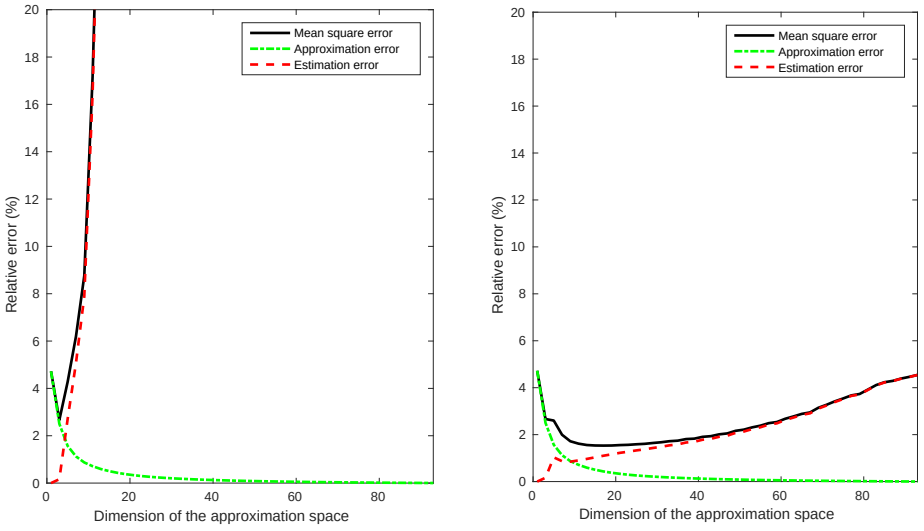

(a) (b)

Fig. 2: Errors obtained (a) without and (b) with penalization.

this dimension, the MSE quickly went above 20% without penalization while it remained below 5% until the highest dimension with penalization. As a conclusion, without penalization, it was not possible to estimate correctly coefficients of high-frequency components of the topothesy. Such an estimation could be accurately achieved with a penalization, showing the benefit of the proposed method.

H	$[0.05, 0.2)$	$[0.2, 0.35)$	$[0.35, 0.5)$	$[0.5, 0.65)$	$[0.65, 0.8)$	$[0.8, 0.95)$	$[0.95, 1)$
Error (%)	0.93	1	1.34	1.82	2.5	2.9	3.88

Table 1: Errors as a function of the Hurst index.

To further analyse results of the penalization method, we computed MSE with an approximation dimension of 39 ($A = 19$) by range of Hurst index values H; see Table 1. The Hurst index had an effect on the estimation performance. When it was close to 1, the MSE was large. In this case, the condition number κ of the matrix $L^T L$ was large, leading to a strong penalization and a high estimation bias (see Theorem 3 and Corollary 1). However, when H was not too large (< 0.65) the MSE was moderate ($< 2\%$). Hence, in such a situation, we could obtain good estimates of high frequency components of the topothesy.

5. An application photographic papers

In this section, we present an application to historical photographic prints. The texture of these prints is a feature which is critical for the works of artists, manufacturers, and conservators [19, 24]. In particular, conservators rely upon the texture to investigate the origin of an unknown print [19]. At present, such investigations are manually done by comparing the texture of the unknow print to those of identified references. They could be eased by an automated classification tool that would select relevant references and measure texture similarities between prints. To test the feasibility of automated classifications of historic photographic paper, two conservators named P. Messier and R. Johnson assembled two datasets [19, 24]. The first one, named the inkjet dataset, gathers 120 photomicrographs of non-printed inkjet papers collected from the Whilhelm Analog and Digital Color Print Material Reference Collection [24]. The second one, named the b&w dataset, is composed of 120 photomicrographs of non-printed silver gelatin photographic papers [19]. These datasets are publicly available at www.PaperTextureID.org. Some classification attempts were reported in conference papers [2, 21, 26, 32, 34].

They are both organized into 4 groups containing sample sets of an increasing heterogeneity. In group 1, there are 3 sets of 10 samples obtained from a same sheet and expected by experts to have a high degree of similarity. In group 2, there are 3 sets of 10 samples from different sheets of a same manufacturer package which should also show a strong similarity albeit to a lesser extent. In group 3, there are 3 sets of 10 samples made from same manufacturer specifications over time and expected to be more dissimilar. The group 4 is composed of 30 samples selected to show the diversity of papers. Datasets are documented in [19, 24] with meta-data including manufacturer, brand, date, type of texture and reflectance.

Photomicrographs of these datasets were acquired using a microscope system under the illumination of a single light placed at a 25 degree raking angle to the surface of the paper [19, 24]. This specific illumination produces highlights and shadows reflecting reliefs of the paper surfaces (see examples in Figures 3 and 4). Depending on the paper properties, image textures look more or less rough and anisotropic. So as to characterize these paper properties, we used two texture features derived from our estimation procedure: the Hurst index H and an anisotropy index I defined as

$$I = \sqrt{\int_{[0,\pi)} \left(\tau^*(s) - \int_{[0,\pi)} \tau^*(u) du \right)^2 ds}. \tag{35}$$

These indices were computed by replacing H and τ^* by their estimate (see Section 3.2). Let

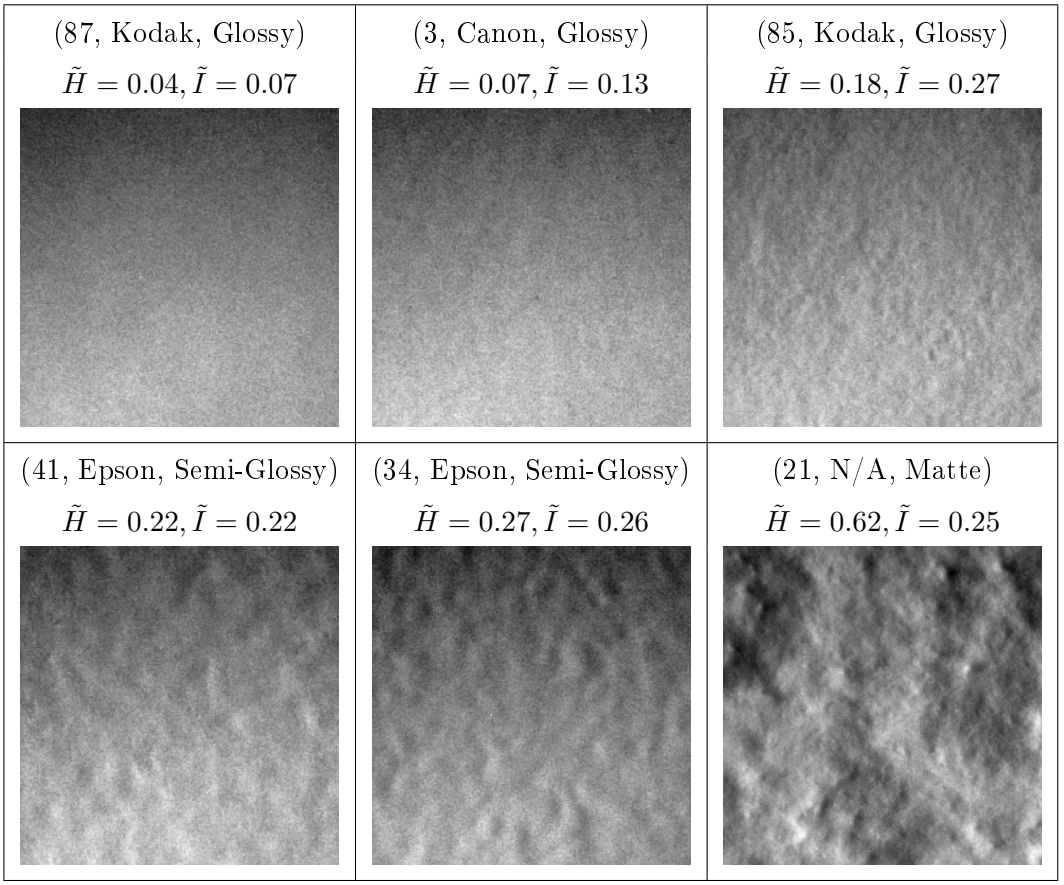

Fig. 3: Patches of size 500×500 extracted from the inkjet dataset, associated to their metadata (sample number, manufacturer, reflectance) and computed indices $\tilde{H}$ and $\tilde{I}$.

us notice that the estimated topothesy was normalized. Consequently, the anisotropy index was invariant to both the field variance and the increment filter used for the estimation.

For the estimation of the Hurst index and the topothesy, we computed quadratic variations using a mono-directional increment filter of the form (17). The length L of the filter was adapted to each image so that increments satisfy conditions of Theorem 2. It was set to $L = M + 2$ (filter of order $M + 1$) using an estimate M of the order of the IRF underlying the image. This order M was taken as the lowest one for which quadratic variations of image increments became almost constant at large scales. For most of the images, the maximal scale at which increments were computed was set to 20 pixels. But, for some papers (*e.g.* glossy inkjet papers), the relationship between logarithms of quadratic variations and scales was poorly linear at scales above 7 pixels. So, for these papers, the maximal scale was automatically set to 7 pixels. Between minimal and maximal scales, we used all possible increments in directions where at least two increments could be com-

puted. Using quadratic variations of these increments, we estimated parameters of the linear model (19), including the Hurst index and the intercepts β. Using scales below 20 pixels (resp. 7 pixels), we could estimate intercepts in 96 (resp. 17) directions. Using these estimates, we set the procedure for the estimation of the topothesy function. In this procedure, the parameter A was set to 23 (resp. 2) so to ensure that the dimension $2A+1$ of the approximation space was about the half of the number of intercepts.

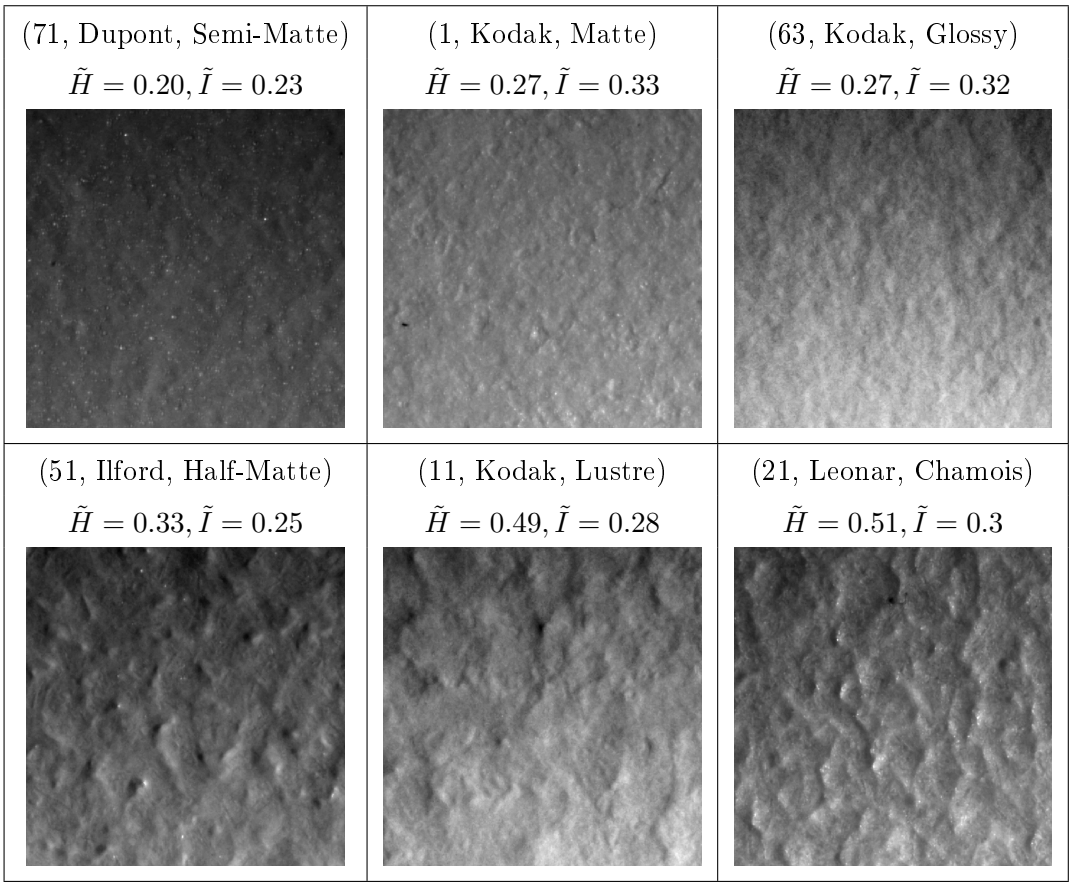

Fig. 4: Patches of size 500×500 extracted from papers of the b&w dataset, associated to their metadata (sample number, manufacturer, reflectance) and computed indices $\tilde{H}$ and $\tilde{I}$.

On Figures 5 and 6, we ploted couples ($\tilde{H}$,$\tilde{I}$) of textures of groups 1 to 3 for inkjet and b&w datasets. For textures of group 1 ("same sheet") and 2 ("same package") of the inkjet dataset, indices were both homogeneous within each set and separated across sets, showing a stability of the manufacturing process. Sets 61-70 and 71-80 of group 3 ("same manufacturer") were also quite homogeneous, but not the set 81-90. The variability of this set could be due to the variety of paper brands. Besides, we observed three point clusters

corresponding to papers with a same reflectance: A first cluster composed of glossy papers with low Hurst and anisotropy indices, a second one containing semi-glossy papers with larger Hurst and anisotropy indices, and a third one formed by matte papers with larger Hurst indices. Some samples of these clusters are shown on Figure 3 with their associated indices.

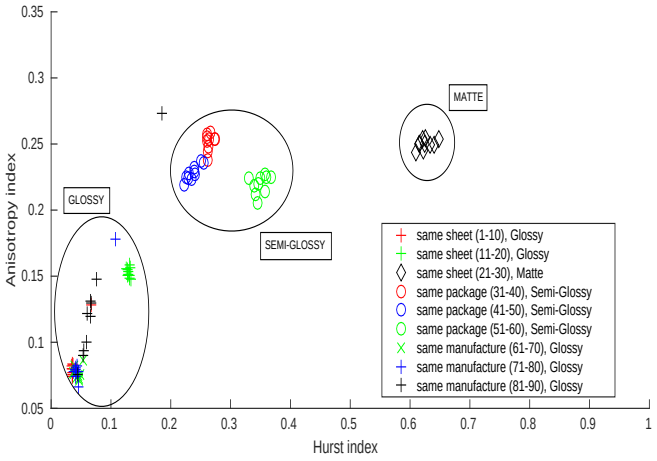

Fig. 5: Hurst and anisotropy indices of texture samples of different groups from the inkjet dataset.

Textures of the b&w dataset showed a larger intra-set variability than those of the inkjet dataset, even for papers of groups 1 and 2. Textures of these photographic papers might be less homogeneous than the inkjet ones. The variability was particularly large on the set 81-90 of group 3. This was probably due to the variety of paper reflectance within this set. On the b&w dataset, we also observed three main clusters corresponding to groups of papers with common reflectance. A first cluster included the semi-matte and glossy papers (low Hurst and anisotropy indices), a second one the matte and glossy papers (low Hurst index and large anisotropy index), and a third one the lustre, champois and half-matte papers (large Hurst and anisotropy indices). Papers from these different clusters are compared on Figure 4.

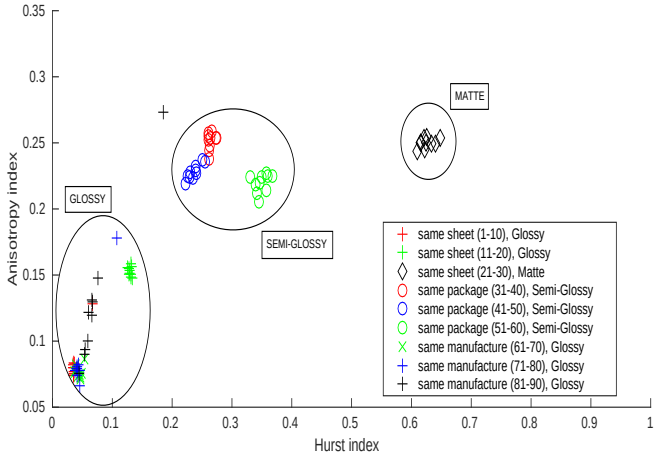

Fig. 6: Hurst and anisotropy indices of texture samples of different groups from the b&w dataset.

For each sample pair, we further determined a degree of affinity ranging in five levels from "very poor" to "perfect". This level of affinity was computed by thresholding the euclidean distance between index values $(\tilde{H}, \tilde{I})$ of samples. In this procedure, thresholds were automatically set to optimize over a whole dataset the matching between the computed affinities and the ones established by an expert from meta-data. In Figure 7, we display in the form of a matrix the sample affinities computed for each dataset and compare them to the expert ones.

The affinity between inkjet papers of a same group was globally well estimated at level excellent, except for the group 81-90 (papers of the manufacturer Kodak). The level of affinity between glossy papers (sets 1-10 and 61-90) and semi-glossy papers (sets 31-60), which is considered as good by experts, was underestimated at level fair or poor. The affinity between glossy papers (sets 1-10 and 61-90) and matte papers (set 21-30) was correctly estimated at level very poor whereas the one between semi-glossy papers (sets 61-90) and matte papers was slight overestimated at level poor. The affinity between glossy papers of different brands (Canon: 1-10, HP: 61:70, Epson: 71-80, Kodak: 81-

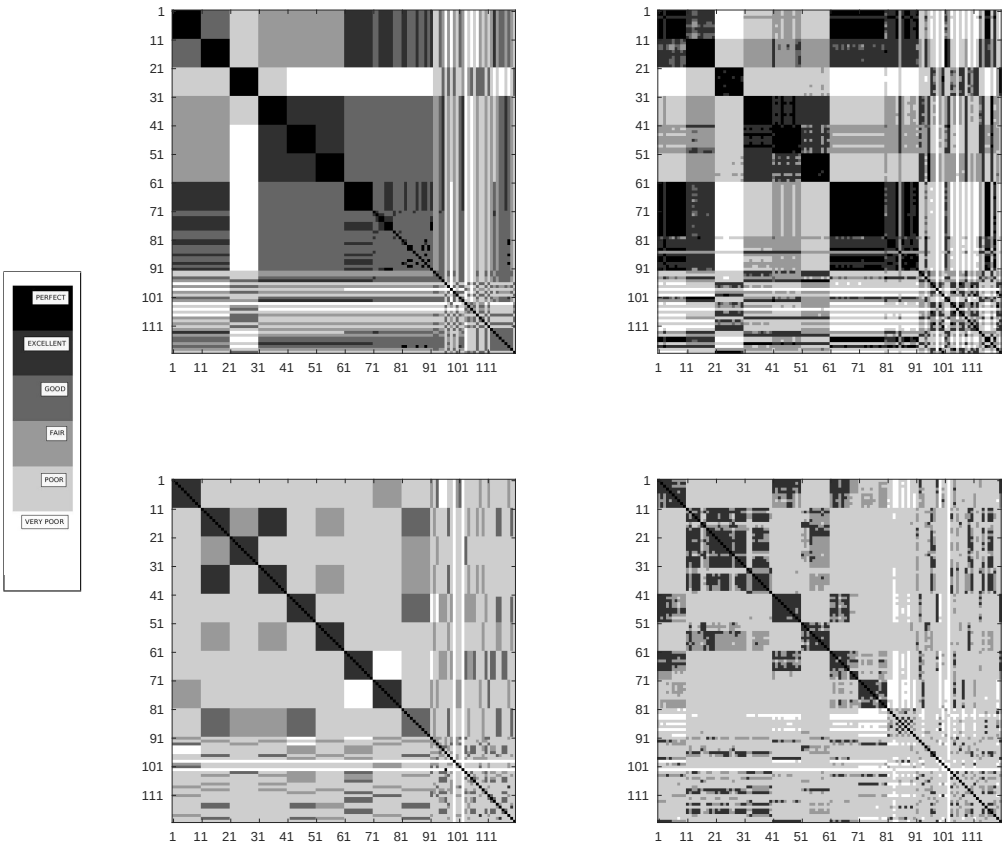

Fig. 7: Affinity matrices from experts (left) and computations (right) for the inkjet dataset (top) and b&w dataset (bottom).

90) was mostly estimated at levels excellent or perfect whereas it is only qualified as good by experts. Globally, the affinity matrices obtained by experts and the automated classification matched at a level of 40%.

The affinity between b&w papers of a same group was well-estimated at level good or excellent, except for the group 81-90 which mixes glossy and lustre papers. The affinity evaluated as poor by experts were globally well-estimated. This is for instance the case between glossy papers of Ilford group 41-50 and lustre papers from Kodak groups 11-20 and 31-40. Some affinities qualified as good by experts were underestimated at levels poor or very poor between the lustre and glossy papers of the group 81-90 and groups 11-20, 41-50. For b&w papers, the overall match between affinity matrices obtained by experts and the automated classification was of 60%.

6. Discussion

We presented an approach for the characterization of the anisotropy of Holder random fields. Using the field spectral density, we first defined an asymptotic notion of topothesy which quantifies the directional contributions of high-frequencies to the field irregularity. We then designed and evaluated a procedure based on multi-oriented quadratic variations for the estimation of this asymptotic topothesy. Eventually, we used this procedure for the classification of textures of photographic papers. This classification was done by combining two features, a usual estimate of the Holder index of the field and a new anisotropy index derived from the estimated asymptotic topothesy. It led to some clusters gathering papers with similar reflectances.

The anisotropy index we used are related to the ones proposed in [27, 28]. These indices are also obtained from the directional intercept function β_{H,τ^*} that appears in the linear asymptotic relationship between multi-oriented quadratic variations and the Holder index of the field (see Equation (20) of Theorem 2). They measure a dispersion of the intercept function and, indirectly, of the asymptotic topothesy. However, they depend on the Holder index of the field and the order of increments required for its analysis (this order has to be set with respect to the order of the field). Hence, their variations do not exclusively reflect differences between field directional properties. They also account for changes of field regularity or order. By contrast, the anisotropy index of this paper is a direct measure of dispersion of the asymptotic topothesy. This measure is intrinsically related to directional properties of the field and invariant to its order and Holder index.

For the classification, information carried by the asymptotic topothesy was reduced to a

single anisotropy index, but it is much richer. Depending on the interest for the application, other indices such as kurtosis or skewness of the asymptotic topothesy could be computed. Directions where the asymptotic topothesy reaches optima could also be of interest for finding main orientations of an image texture. Besides, according to Proposition 2, the asymptotic topothesy provides us with an information about the correlation structure of field high-frequencies. Such an information could be used to set an IRF model where the image would be decomposed into a trend field and a texture field with a specified correlation structure. Using such a model, it would become possible to achieve other image processing tasks such as separation of trend and texture of an image, examplar-based texture simulations, or inpainting of missing or occluded parts of an image.

References

[1] P. Abry, M. Clausel, S. Jaffard, S. Roux, and B. Vedel. Hyperbolic wavelet transform: an efficient tool for multifractal analysis of anisotropic textures. *Rev. Mat. Iberoam.*, 31(1):313–348, 2015.

[2] P. Abry, S. Roux, H. Wendt, P. Messier, et al. Multiscale anisotropic texture analysis and classification of photographic prints. *IEEE Signal Process. Mag.*, 32(4):18–27, 2015.

[3] R. Adler. *The geometry of random fields*, volume 62. SIAM, 2010.

[4] D. Benson, M. M. Meerschaert, B. Bäumer, and H. P. Scheffler. Aquifer operator-scaling and the effect on solute mixing and dispersion. *Water Resour. Res.*, 42:1–18, 2006.

[5] H. Biermé. *Champs aléatoires : autosimilarité, anisotropie et étude directionnelle.* PhD thesis, University of Orleans, France, 2005.

[6] H. Biermé, C.L. Benhamou, and F. Richard. Parametric estimation for Gaussian operator scaling random fields and anisotropy analysis of bone radiograph textures. In K. Pohl, editor, *Proc. of MICCAI*, pages 13–24, London, UK, september 2009.

[7] H. Biermé and C. Lacaux. Hölder regularity for operator scaling stable random fields. *Stoch. Proc. Appl.*, 119(7):2222–2248, 2009.

[8] H. Biermé, M. M. Meerschaert, and H. P. Scheffler. Operator scaling stable random fields. *Stoch. Proc. Appl.*, 117(3):312–332, 2007.

[9] H. Biermé, M. Moisan, and F. Richard. A turning-band method for the simulation of anisotropic fractional Brownian field. *J. Comput. Graph. Statist.*, 24(3):885–904, 2015.

[10] H. Biermé and F. Richard. Analysis of texture anisotropy based on some Gaussian fields with spectral density. In M. Bergounioux, editor, *Mathematical Image Processing*, pages 59–73. Springer Proc., 2011.

[11] H. Biermé and F.J.P. Richard. Estimation of anisotropic Gaussian fields through Radon transform. *ESAIM: Probab. Stat.*, 12(1):30–50, 2008.

[12] A. Bonami and A. Estrade. Anisotropic analysis of some Gaussian models. *J. Fourier Anal. Appl.*, 9:215–236, 2003.

[13] G. Chan and T.A. Wood. Increment-based estimators of fractal dimension for two-dimensional surface data. *Stat. Sinica*, 10:343–376, 2000.

[14] J.P. Chilès and P. Delfiner. *Geostatistics: modeling spatial uncertainty*. J. Wiley, 2nd edition, 2012.

[15] M. Clausel and B. Vedel. Explicit construction of operator scaling Gaussian random fields. *Fractals*, 19(01):101–111, 2011.

[16] S. Davies and P. Hall. Fractal analysis of surface roughness by using spatial data. *J. Roy. Statist. Soc. Ser. B*, 61:3–37, 1999.

[17] I.M. Gelfand and N. Ya. Vilenkin. *Generalized functions*, volume 4: Applications to harmonic analysis. Academic Press, 1964.

[18] R. Hochmuth. Wavelet characterizations for anisotropic Besov spaces. *Appl. Comput. Harmon. Anal.*, 12(2):179–208, 2002.

[19] R. Johnson, P. Messier, W. Sethares, et al. Pursuing automated classification of historic photographic papers from raking light images. *J. Am. Inst. Conserv.*, 53(3):159–170, 2014.

[20] L. Kaplan and C.-C. Jay Kuo. Texture roughness analysis and synthesis via extended self-similar (ESS) model. *IEEE Trans. Pattern Anal. Mach. Intell.*, 17(11):1043–1056, 1995.

[21] A. Klein, A. Do, C. Brown, and P. Klausmeyer. Texture classification via area-scale analysis of raking light images. In *IEEE Asilomar Conf. on Signals, Systems and Computers*, pages 1114–1118, 2014.

[22] B. B. Mandelbrot and J. Van Ness. Fractional Brownian motion, fractionnal noises and applications. *SIAM Rev.*, 10:422–437, 1968.

[23] G. Matheron. The intrinsic random functions and their applications. *Ad. Appl. Prob.*, 5:439–468, 1973.

[24] P. Messier, R. Johnson, H. Wilhelm, W. Sethares, A. Klein, et al. Automated surface texture classification of inkjet and photographic media. In *NIP & Digital Fabrication Conference*, pages 85–91. Society for Imaging Science and Technology, 2013.

[25] A. Pentland. Fractal-based description of natural scenes. *IEEE Trans. Pattern Anal. Mach. Intell.*, 6:661–674, 1984.

[26] D. Picard, N.-S. Vu, and I. Fijalkow. Photographic paper texture classification using model deviation of local visual descriptors. In *IEEE Int. Conf. on Image Processing*, pages 5–p, 2014.

[27] F.J.P. Richard. Analysis of anisotropic Brownian textures and application to lesion detection in mammograms. *Procedia Environ. Sci.*, 27:16–20, 2015.

[28] F.J.P. Richard. Some anisotropy indices for the characterization of Brownian textures and their application to breast images. *Spat. Stat.*, 18:147–162, 2016.

[29] F.J.P. Richard. Tests of isotropy for rough textures of trended images. *Stat. Sinica*, 26(3):1279–1304, 2016.

[30] F.J.P. Richard and H. Biermé. Statistical tests of anisotropy for fractional Brownian textures. Application to full-field digital mammography. *J. Math. Imaging Vis.*, 36(3):227–240, 2010.

[31] S. Roux, M. Clausel, B. Vedel, S. Jaffard, and P. Abry. Self-similar anisotropic texture analysis: The hyperbolic wavelet transform contribution. *IEEE Trans. Image Process.*, 22(11):4353–4363, 2013.

[32] S. Roux, N. Tremblay, P. Borgnat, P. Abry, H. Wendt, and P. Messier. Multiscale anisotropic texture unsupervised clustering for photographic paper. In *IEEE Int. Workshop on Information Forensics and Security (WIFS)*, pages 1–6, 2015.

[33] M. B. Slimane and H. B. Braiek. Directional and anisotropic regularity and irregularity criteria in Triebel wavelet bases. *J. Fourier Anal. Appl.*, 18(5):893–914, 2012.

[34] N. Tremblay, S. Roux, P. Borgnat, P. Abry, H. Wendt, and P. Messier. Texture classification of photographic papers: improving spectral clustering using filterbanks on graphs. In *Proc. GRETSI Symposium Signal and Image Processing*, Lyon, France, 2015.

A. Proofs

Proof (Proposition 2). For some positive constant c, we have

$$\Delta_A(x) = |K_{A,f}(x) - K_{A,f^*}(x)| \leq c \int_{|w|\geq A} |f(w) - f^*(w)| dw.$$

Since the field density satisfies Condition (6), we further obtain

$$\begin{aligned}
\Delta_A(x) &\leq c \int_{|w|\geq A} |f(w) - g_{\tau,\eta}(w)| dw + \int_{|w|\geq A} |f^*(w) - g_{\tau,\eta}(w)| dw, \\
&\leq \tilde{c} \int_{|w|\geq A} |w|^{-2H-d-\gamma} dw + \int_{|w|\geq A} |f^*(w) - g_{\tau,\eta}(w)| dw, \\
&\leq o(A^{-2H}) + \int_{|w|\geq A} |f^*(w) - g_{\tau,\eta}(w)| dw,
\end{aligned}$$

as A tends to $+\infty$.

Now, in directions s of the set $E_0 = \{s, \tau^*(s) > 0\}$, we notice that $\eta(s) = H$ and $\tau^*(s) = \tau(s)$. Hence, $f^*(w) = g_{\tau,\eta}(w)$ whenever $\arg(w)$ is in E_0, $f^*(w) = g_{\tau,\eta}(w)$, and 0 otherwise. Consequently, in polar coordinate, we have

$$\begin{aligned}
\int_{|w|\geq A} |f^*(w) - g_{\tau,\eta}(w)| dw &= \int_{E_0^c} \int_A^{+\infty} g_{\tau,\eta}(\rho s) \rho^{d-1} d\rho \, ds, \\
&\leq c \int_{E_0^c} \int_A^{+\infty} \rho^{-2\eta(\theta)-1} d\rho \, ds.
\end{aligned}$$

Then, let us decompose the integral over E_0^c into the sum of two integrals, one over a set $F_\delta = \{s, \eta(s) - H > \delta/2\}$ defined for $\delta > 0$, and the other over a set $E_\delta = \{s, 0 < \eta(s) - H < \delta/2\}$. It follows that

$$\int_{|w|\geq A} |f^*(w) - g_{\tau,\eta}(w)| dw = O(A^{-2H})(A^{-\delta} + \mu(F_\delta)).$$

where $\mu(F_\delta)$ is the measure of F_δ on the unit sphere of $\mathbb{R}^d$. But, as shown in [29], $\lim_{\delta\to 0} \mu(F_\delta) = 0$. Hence, letting $\delta = \log(A)^{1-\alpha}$ for some $0 < \alpha < 1$, we obtain

$$\int_{|w|\geq A} |f^*(w) - g_{\tau,\eta}(w)| dw = o(A^{-2H}).$$

Consequently, $\Delta_A(x) = o(A^{-2H})$ as A tends to $+\infty$.

PROOF (PROPOSITION 3). When the increment field is mono-directional, the expression of $\Gamma_{H,v}$ of Equation (21) reduces to

$$\Gamma_{H,v}(\theta) = \int_{\mathbb{R}^+} |\hat{v}_1(\rho\cos(\theta))|^2 \rho^{-2H-1} d\rho.$$

The expression of β_{H,τ^*} in Equation (26) follows from the simple coordinate change $u = \rho\cos(\theta)$.

PROOF (THEOREM 3). We aim at estimating the solution τ^* of a linear system $L_H\,\tau = \beta$ with a random vector

$$\tilde{\tau}^*_\lambda = (L_H^T L_H + \lambda R)^{-1}\tilde{\beta}$$

where R is a diagonal matrix, $\lambda > 0$, and $\tilde{\beta}$ is an unbiased estimate of β of variance $V(\beta)$.

Since $\tilde{\beta}$ is unbiased, the expectation of $\tilde{\tau}^*_\lambda$ satisfies

$$(L_H^T L_H + \lambda R)\mathbb{E}(\tilde{\beta}) = L_H^T \beta,$$

so that

$$(L_H^T L_H + \lambda R)(\mathbb{E}(\tilde{\beta}) - \tau^*) = -\lambda R\tau.$$

Thus,

$$|\mathbb{E}(\tilde{\beta}) - \tau^*|_2 = |(L_H^T L_H + \lambda R)^{-1}\lambda R\tau|_2,$$

where $|\cdot|_2$ denotes the 2-norm. Hence, using norm properties, we get

$$|\mathbb{E}(\tilde{\beta}) - \tau^*|_2 \leq \lambda |(L_H^T L_H + \lambda R)^{-1}|_2\, |R|_2\, |\tau|_2.$$

We further have

$$\begin{aligned}\frac{|\mathbb{E}(\tilde{\beta}) - \tau^*|_2}{|\tau|_2} &\leq \lambda |(L_H^T L_H)^{-1}|_2\, |(I + \lambda (L_H^T L_H)^{-1} R)^{-1}|_2\, |R|_2 \\ &\leq \frac{\lambda(2A+1)}{\nu_-}\, |(I + \lambda (L_H^T L_H)^{-1} R)^{-1}|_2, \end{aligned} \tag{36}$$

where ν_- is the lowest eigenvalue of $L_H^T L_H$ and $2A+1$ the highest term of the diagonal of R. Next, we establish a bound for $|(I + \lambda (L_H^T L_H)^{-1} R)^{-1}|_2$. Let u be a vector, we have

$$\begin{aligned}|(I + \lambda (L_H^T L_H)^{-1} R)u|_2^2 &= |(I + \lambda (L_H^T L_H)^{-1} + \lambda (L_H^T L_H)^{-1}(R - I))u|_2^2, \\ &\geq |(I + \lambda (L_H^T L_H)^{-1})u|_2^2 + 2\lambda a(u,u),\end{aligned}$$

where $a(u,u) = u^T((L_H^T L_H)^{-1} + \lambda (L_H^T L_H)^{-2})(R - I)u$. Since $R - I$ is diagonal with non-negative diagonal terms, we have

$$a(u,u) = ((R-I)^{\frac{1}{2}}u)^T((L_H^T L_H)^{-1} + \lambda (L_H^T L_H)^{-2})(R-I)^{\frac{1}{2}}u.$$

Moreover, the matrix $(L_H^T L_H)^{-1} + \lambda (L_H^T L_H)^{-2}$ has eigenvalues $\alpha + \lambda \alpha^2$ defined with eigenvalues α of $(L_H^T L_H)^{-1}$. Hence, this matrix is definite positive. Therefore, $a(u,u) \geq 0$ and

$$|(I + \lambda (L_H^T L_H)^{-1} R)u|_2^2 \geq |(I + \lambda (L_H^T L_H)^{-1})u|_2^2.$$

Consequently,

$$|I + \lambda (L_H^T L_H)^{-1} R|_2 \geq |I + \lambda (L_H^T L_H)^{-1}|_2 = (1 + \frac{\lambda}{\nu_-}).$$

Thus,

$$|(I + \lambda (L_H^T L_H)^{-1} R)^{-1}|_2 \leq \frac{\nu_-}{(\nu_- + \lambda)}. \tag{37}$$

Using Equation (36), we eventually obtain the inequality (32).

Now, we turn to the variance of the estimator, which is defined as

$$V(\tilde{\tau}_\lambda^*) = \mathbb{E}\left((\tilde{\tau}_\lambda^* - \mathbb{E}(\tilde{\tau}_\lambda^*))(\tilde{\tau}_\lambda^* - \mathbb{E}(\tilde{\tau}_\lambda^*))^T\right).$$

We have

$$\text{trace}(V(\tilde{\tau}_\lambda^*)) = \text{trace}\left(((L_H^T L_H) + \lambda R)^{-1} L_H^T V(\tilde{\beta}) L_H ((L_H^T L_H) + \lambda R)^{-1}\right).$$

Then, using the fact that any term $V(\tilde{\beta})_{ij}$ of $V(\tilde{\beta})$ is bounded by $\sqrt{V(\tilde{\beta})_{ii} V(\tilde{\beta})_{jj}}$, we obtain

$$\text{trace}(V(\tilde{\tau}_\lambda^*)) \leq |((L_H^T L_H) + \lambda R)^{-1} L_H^T \Delta|_2^2 \leq |((L_H^T L_H) + \lambda R)^{-1} L_H^T|_2^2 \, |\Delta|_2^2,$$

where Δ is a vector formed by terms $\sqrt{V(\tilde{\beta})_{ii}}$. Next, we notice that $|\Delta|_2^2 = \text{trace}(V(\tilde{\beta}))$, and

$$|((L_H^T L_H) + \lambda R)^{-1} L_H^T \Delta|_2^2 \leq |(L_H^T L_H)^{-1}|_2^2 |(I + \lambda (L_H^T L_H)^{-1} R)^{-1}|_2^2,$$

Hence, using Equation (37), we get

$$\sqrt{\text{trace}(V(\tilde{\tau}_\lambda^*))} = \frac{1}{\nu_- + \lambda} \sqrt{\text{trace}(V(\tilde{\beta}))}.$$

Besides, since $L_H^T L_H \tau^* = L_H^T \beta$, we have

$$|L_H^T L_H|_2 \, |\tau^*|_2 \geq |L_H^T \beta|_2 \geq \sqrt{\nu_-} |\beta|_2.$$

Hence,

$$\frac{1}{|\tau^*|_2} \leq \frac{\nu_+}{\sqrt{\nu_-} |\beta|_2},$$

and the inequality (33) follows.

Proof (Corollary 1). Using expressions of bias and variance in Theorem 3, we clearly see that the function g bounds the relative mean square error. Then, a simple variation analysis of this function suffices to show that it reaches a global minimum at λ^*.